ACS Sustainable Chemistry & Engineering

pubs.acs.org/journal/ascecg

Research Article

Discovery of Piezoelectricity in Natural Birch Bark for AI-Assisted Sports Violation Monitoring

Biyao Huang, Chu Pan, Xueyi Li, Juan Li, Weiqing Yang,* and Jun Lu*,#

Cite This: ACS Sustainable Chem. Eng. 2026, 14, 8331−8341

Read Online

ACCESS | Metrics & More | Article Recommendations | Supporting Information

ABSTRACT: The rapid advancement of wearable electronics has created an urgent demand for distributed, sustainable, and green energy sources to power various microdevices. As the conventional lithium battery is harmful to the environment, the biopiezoelectric nanogenerator is an ideal candidate to meet these requirements. Here, we develop a piezoelectric nanogenerator based on natural birch bark derived from *Betula platyphylla*, which exhibits a piezoelectric coefficient (d_{33}) of 3.09 pm V^{-1}, a piezoelectric voltage output of 29.3 V cm^{-3}, a piezoelectric current output of 0.33 μA cm^{-3}, and a power density of 3.42 μW cm^{-3}. After over 10,000 cycles of mechanical impact or 180 days of storage, its piezoelectric output shows no significant degradation, confirming robust electromechanical conversion. As a proof of concept, an integrated sports violation recognition system is further designed by combining a birch-bark piezoelectric nanogenerator with a multilayer perceptron classifier. With the assistance of machine learning, the system can accurately identify rule violations, offering reliable technical support for referees. This study provides a new way of fabricating self-powered green micro/nanodevices in the Era of Artificial Intelligence, paving the way for sustainable energy solutions in smart electronics.



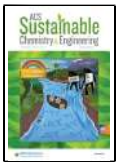
KEYWORDS: *birch bark, cellulose, piezoelectric nanogenerator, sports violation monitoring, machine learning*

INTRODUCTION

The rising popularity of smart wearable and portable electronic devices has created an urgent demand for distributed, sustainable, and green energy sources to power various microdevices.[1−5] The direct piezoelectric effect, which converts ambient mechanical energy into electricity, therefore, represents a highly promising route for energy harvesting. A key advantage over thermal or solar sources lies in the typically continuous or controllable nature of vibrations, minimizing the dependence on variable environmental conditions. The traditional piezoelectric materials comprise inorganic piezoelectric materials (e.g., lead zirconate titanate (PZT)[6] and barium titanate (BTO)[7]), as well as organic piezoelectric materials (e.g., polyvinylidene fluoride (PVDF)[8]). However, their intrinsic toxicity, inadequate ecofriendliness, poor biocompatibility, and limited degradability hinder environmental sustainability. Interestingly, many biological materials possess highly ordered structures with low symmetry and no inversion center, making linear electromechanical coupling an inherent property of various biomolecules.[9]

To date, most reported biopiezoelectric nanogenerators (BPNGs) are based on proteins and polysaccharides, whose piezoelectricity originates from the molecular structure and orientation of the polymers.[10] Among these, collagen, the most abundant structural protein in animals, is widely distributed in the bones, skin, and muscles. The collagen exhibits piezoelectricity due to the accumulation of dipoles along peptide chains and hydrogen bonds in supramolecular packing.[11] Previously reported collagen-based BPNGs include those based on eggshell membrane,[12] fish scales,[13] pollock skin,[14] and others. In addition, keratin, which possesses piezoelectricity originating from the oriented conformations of α-helices or β-sheets and intramolecular disulfide bond cross-linking, has been utilized in BPNGs, with examples such as snake ecdysis[15] and chicken feather fibers.[16] For polysaccharides, the main candidates are cellulose and chitosan. Research on the piezoelectricity of cellulose dates back to 1955, when the piezoelectric effect of wood was first discovered;[17] to date, relevant studies have been reported on these materials including onionskin,[18] ginkgo leaves,[19] date fruit membrane,[20] and pomelo fruit membrane.[21] Owing to their remarkable biocompatibility, biodegradability, high flexibility, and low cost, these biopiezoelectric materials have been extensively utilized for fabricating biopiezoelectric energy harvesters. In previous studies on the piezoelectricity of wood, natural wood has generally been reported to exhibit weak piezoelectric properties.[22−24] However, we note that it has been proposed that the piezoelectric modulus exhibits a gradual increase from the trunk to the bark.[25] Thus, we consider birch bark derived from

Received: January 22, 2026
Revised: April 10, 2026
Accepted: April 13, 2026
Published: April 17, 2026



ACS Publications

© 2026 American Chemical Society

https://doi.org/10.1021/acssuschemeng.6c00906
ACS Sustainable Chem. Eng. 2026, 14, 8331−8341

Downloaded from pubs.acs.org/ascecg/article-pdf/14/17/8331/6820526/sc600906.pdf by SOUTHWEST JIAOTONG UNIV user on 07 November 2026

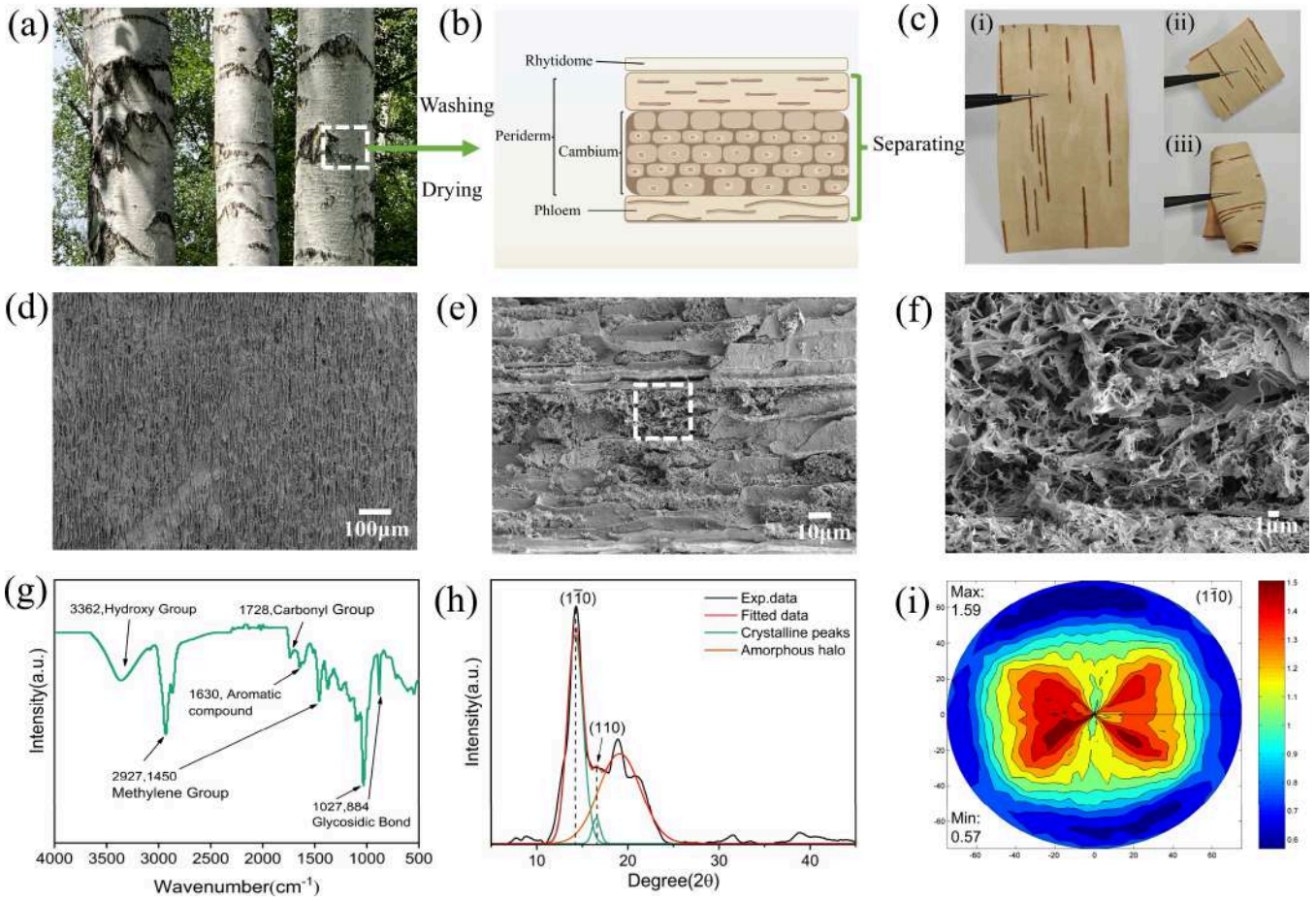


Figure 1. (a) Photograph of *Betula platyphylla*. (b) Schematic of the layered structure of birch bark (BB) derived from *Betula platyphylla*. (c) Photograph of (i) BB, (ii) folded, and (iii) rolled BB presenting its flexibility. (d) SEM micrograph of the BB surface. (e) SEM micrograph of the BB cross-section. (f) Magnified SEM image of the BB cross-section. (g) FTIR spectrum of the BB. (h) XRD analysis of the BB. (i) Pole figure of the cellulose (1$\bar{1}$0) plane in natural BB.

Betula platyphylla, a naturally abundant biological material, as a piezoelectric material that exhibits sustainability, biodegradability, and piezoelectric properties. To the best of our knowledge, the piezoelectric characteristics of natural bark-based piezoelectric nanogenerators have not been reported to date.

Betulaceae is an important taxon within angiosperms, and Betula (birch) is the largest genus in this family, with 119 recognized species identified to date.[26] One of these species, distributed in Russia, Japan, and Northeast China, is referred to as *Betula platyphylla* (white birch), which is often portrayed as a symbol of tenacity, purity, and vitality in works of art. In Russia, *Betula platyphylla* forests account for over 40% of the total forest area.[27] Compared to other birch species, the *Betula platyphylla* possesses exceptional cold hardiness by regulating the activity of antioxidant enzymes, capable of withstanding temperatures as low as −70 °C.[28−30] Its growth in extremely cold environments contributes to higher wood density,[31] rendering it more durable and highly processable. Furthermore, wood density is closely associated with the water absorption capacity of wood; higher density also enhances the material's resistance to decay and insect infestation.[32] Birch bark, as a byproduct of wood, is produced in large quantities as a waste product in the sulfate pulp mills. A kraft pulp mill with an annual production capacity of 200,000 tons of pulp produces approximately 14,000 tons of dry weight of outer bark annually.[33] In fact, this bark is mainly burned in biomass boilers for energy recovery or used in crafts and birch tar production. However, incomplete combustion and bark extraction may release pollutants, posing environmental risks. Developing alternative, noncombustion applications could therefore offer significant added value and reduce environmental impacts.

Birch bark has the characteristics of flexibility, renewability, layered structure, waterproofness, and mold resistance.[34−36] Notably, compared to the bark of other tree species, birch bark derived from *Betula platyphylla* exhibits a whiter color and greater smoothness and is more prone to peeling off into numerous large flakes. As a natural biological material, it is primarily composed of cellulose polysaccharides,[37,38] but also contains hundreds of different bioactive components, including triterpenoids (e.g., betulin, betulinic acid, and lupeol), phenolic compounds (e.g., catechol), flavonoids (e.g., quercetin), and tannins, among others.[39−44] Current research predominantly explores the biomedical potential of these extracts, highlighting, for example, the anticancer properties of betulinic acid,[45] the antibacterial and antioxidant effects of catechol.[46] Despite this interest, only a minimal fraction of the birch bark is consumed for medical purposes. Consequently, the vast majority of this resource is currently treated as unutilized biomass waste.

Downloaded from pubs.acs.org/ascecg/article-pdf/14/17/8331/6820526/sc600906.pdf by SOUTHWEST JIAOTONG UNIV user on 07 November 2026

https://doi.org/10.1021/acssuschemeng.6c00906
ACS Sustainable Chem. Eng. 2026, 14, 8331−8341

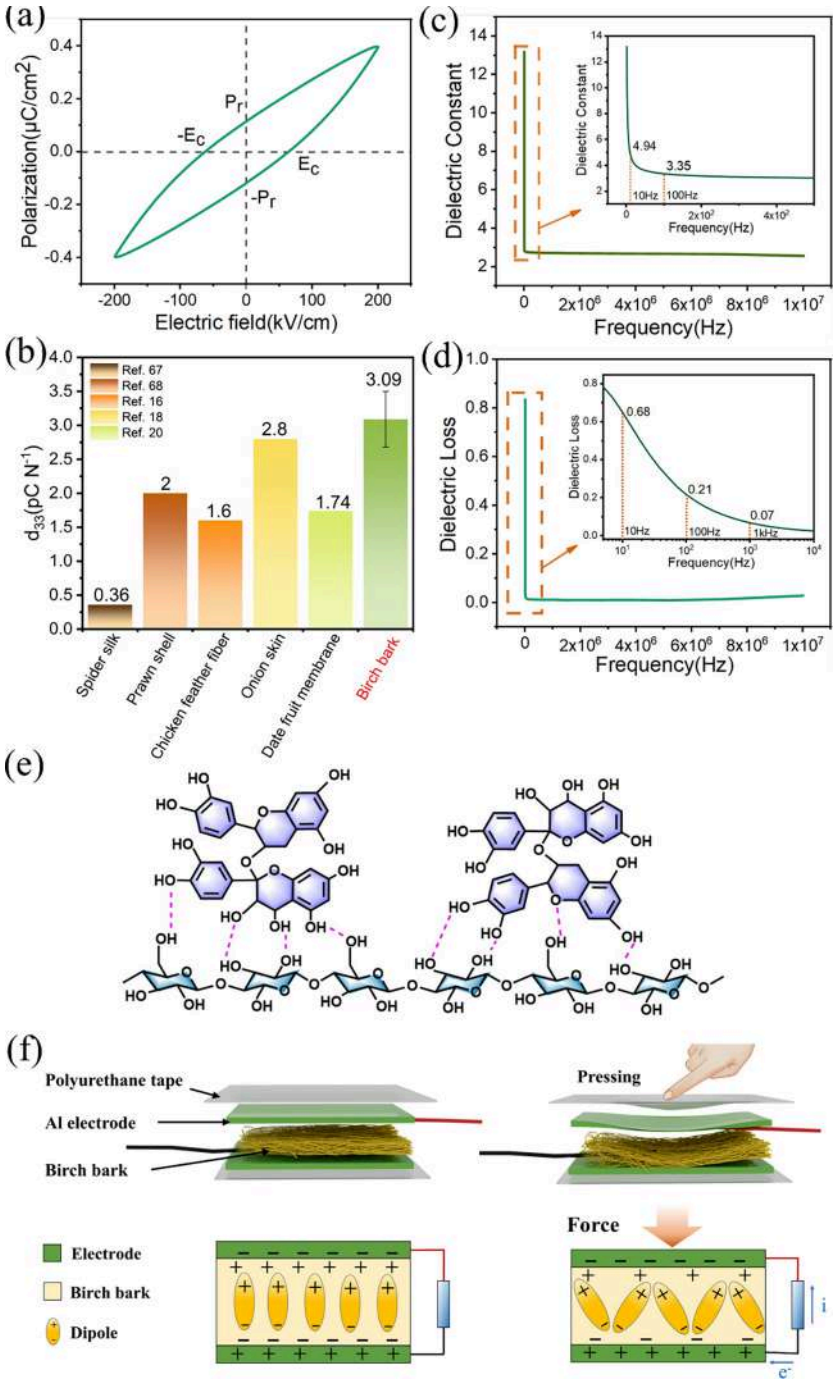


Figure 2. (a) Polarization vs electric field (P−E) curve of an unpoled natural BB. (b) Comparison chart of d_{33} values between untreated natural materials and the BB. (c) Dielectric constant vs frequency curve. (d) Dielectric loss vs frequency curve. (e) Probable intermolecular H-bonding interactions between cellulose and polyphenols (e.g., proanthocyanidins). (f) Schematic diagram of BB-PENG under external force stimulation and the microscopic working mechanism of BB-PENG.

During the upward growth of the birch tree, the cellulose crystals are induced to form a highly preferred orientation within the bark, which presents potential for piezoelectric applications. This study develops a piezoelectric electronic device based on birch bark derived from *Betula platyphylla*, which serves as a fully sustainable, self-polarized piezoelectric material obtained from biological waste. Without any chemical treatment or surface treatment, the birch bark is physically dried and directly used as the piezoelectric active layer to conveniently fabricate an ecofriendly, mechanically flexible, and self-polarized piezoelectric nanogenerator. Utilizing its self-polarized piezoelectric effect, the birch bark-based piezoelectric sensor demonstrates a high piezoelectric output and robust mechanical stability, enabling the detection of subtle joint movements in athletes. As a proof of concept, an integrated violation recognition system is further designed by combining this sensor with a multilayer perceptron (MLP) classifier. With the assistance of machine learning, the system can accurately identify rule violation, offering reliable technical support for referees.

https://doi.org/10.1021/acssuschemeng.6c00906
ACS Sustainable Chem. Eng. 2026, 14, 8331−8341

Downloaded from pubs.acs.org/ascecg/article-pdf/14/17/8331/6820526/sc6c00906.pdf by SOUTHWEST JIAOTONG UNIV user on 07 November 2026

RESULTS AND DISCUSSION

Figure 1a depicts a photograph of *Betula platyphylla*, where the outermost layer features a smooth, white bark with scattered lenticels facilitating gas exchange. The birch bark directly peeled from the *Betula platyphylla* comprises, from outward to inward, the rhytidome, periderm, and phloem sequentially (Figure 1b). During trunk growth, significant pressure is transmitted from the xylem to the cambium and, subsequently, to the bark. Due to the phellem's layered structure, consisting of alternating layers of thick and thin phellem cells, this pressure induces the bark to exfoliate in papery layers. After washing and drying, a multilayered piece of birch bark is obtained. Previous studies have reported that the inner bark exhibits a higher cellulose content than the outer bark.[40] Therefore, the inner bark, which includes the periderm and phloem, was served as the piezo-active layer due to its structural anisotropy (Figure 1c). Its surface displays uniformly distributed, longitudinally oriented ridges and grooves (Figure 1d). Figure 1e,f illustrates the alternating lamellar and fibrous structures. This ordered alternating morphological feature not only contributes to mechanical properties but also provides numerous stress concentration points, thereby enhancing the piezoelectric effect.

Figure 1g presents the Fourier transform infrared (FTIR) spectrum of the natural birch bark. The broad, intense absorption between 3300 and 3400 cm^{-1}, attributable to O−H stretching vibration, confirms the abundance of hydroxyl groups.[47−51] Characteristic peaks for methylene groups ($-CH_2-$) appear at 2927 and 1450 cm^{-1}. The strong band at 1728 cm^{-1} is assigned to C═O stretching in ester groups of suberin, while the peak at 1630 cm^{-1} corresponds to C═C stretches in conjugated carbonyls from aromatic components within suberin and lignin.[49] The peak at 1370 cm^{-1} confirms the presence of alkanes via C−H rocking vibrations. Signals at 1260 and 1160/1100 cm^{-1} represent the C═O stretch in lignin aldehydes and intramolecular C−O/C−C stretches, respectively. Finally, peaks at 1027 and 884 cm^{-1} correspond to C−O stretching and C−O−C deformation of cellulose glycosidic bonds, respectively. Consequently, the IR spectrum confirms that birch bark contains abundant hydroxyl and carbonyl groups as well as ether linkages and aliphatic carbons, consistent with the structures of cellulose, hemicellulose, and lignin. The numerous polar functional groups on natural cellulose molecular chains lay the foundation for dipole formation, while the asymmetric triclinic crystal structure prevents the charge cancellation of the dipoles, thereby promoting the oriented arrangement of molecular chains and resulting in intrinsic molecular dipoles. Furthermore, the hydroxyl groups on the cellulose chains form extensive inter- and intramolecular hydrogen bonds. These bonds promote uniform alignment of molecular dipoles, resulting in a vectorial superposition of dipole moments. Therefore, lattice deformation under external stress yields a net dipole moment change. Notably, the energy-dispersive spectrometer (EDS) elemental mapping confirms the presence of silicon dioxide (Figures S1 and S2). This component mainly derives from the biomineralization process following silica uptake from the soil and thereby reinforces the bark's strength. These elemental mappings corroborate the existence of hydroxyl groups and carbonyl groups in birch bark, which were previously discussed in the FTIR analysis section.

The X-ray diffraction (XRD) spectrum presents the polycrystalline structure of the birch bark (Figure 1h). The diffraction peak at a diffraction angle of 14.39 is a characteristic diffraction signal of the lattice plane of crystalline cellulose, further confirming the presence of cellulose crystals in the birch bark.[52−54] The crystallinity calculated through deconvolution of the XRD pattern (Note S1) is ≈33%, indicating the semicrystalline nature of birch bark. The X-ray pole figure is a direct visualization of crystalline orientation at a given Bragg angle.[55−60] As shown in Figure 1i, the pole figure exhibits a bipolar preferred texture, consisting with the interwoven structure of cellulose microfibrils in birch bark.[61] Moreover, the pole figure reveals a concentrated density distribution at the center, and the calculated maximum pole density reaches 1.59, indicating a high degree of orientation.

It is noteworthy that birch bark contains amorphous components such as lignin and tannins.[62,63] These strong light-absorbing components tend to mask the crystal birefringence signals, thus making untreated birch bark unsuitable for the direct observation of the crystal orientation via polarized optical microscopy (POM). Additionally, the rough surface of birch bark renders it unsuitable for measurements using atomic force microscopy (AFM) or piezoelectric force microscopy (PFM).[64,65] Hence, ferroelectric behavior, which is closely associated with dielectric properties, is pivotal to piezoelectric performance. The spontaneous polarization behavior of birch bark was assessed by measuring the P-E hysteresis loop (Figure 2a). The loop exhibits ferroelectric-like behavior with a residual polarization (P_r) of 0.11 $\mu C\ cm^{-2}$ and a coercive field (E_c) of 60 $kV\ cm^{-1}$. Since stronger crystal alignment usually results in higher remanent polarization, this measured P_r value of 0.11 $\mu C\ cm^{-2}$ is consistent with the moderate-intensity texture corresponding to a maximum pole density of 1.59, reflecting that the piezoelectric domains inside the natural material have achieved partial alignment with a reasonable overall domain orientation degree. Notably, this P_r value is superior to those reported for some other biobased piezoelectric materials, highlighting the advantage of its self-poled nature (Table S1). Furthermore, the piezoelectric performance was quantified by the d_{33} coefficient, which is a critical figure of merit for energy conversion. The unpoled birch bark exhibited a d_{33} of 3.09 $pm\ V^{-1}$ (Note S2). This presents a relatively high value among notable d_{33} coefficients reported for natural piezoelectric materials (Figure 2b and Table S1). The dielectric constant (ε_r) and loss tangent ($\tan\delta$) of birch bark were characterized from 10^{-1} to 10^7 Hz at room temperature using a dielectric analyzer (DEA). As shown in Figure 2c,d, the values at 10 Hz were 4.94 and 0.68, respectively. Both parameters decreased initially with an increasing frequency and then showed relative stability in the high-frequency range (10^5−10^7 Hz). This phenomenon is attributed to the relaxation limitation effect of dielectric polarization.[66] Specifically, the cellulose molecular chains form a highly rigid backbone via β-1,4-glycosidic linkages, while extensive intermolecular hydrogen bonds create a dense network. This structure restricts the mobility of the polar groups, prolonging the dipole orientation polarization time. Consequently, birch bark maintains a stable polarization response under high-frequency electric field excitation. Therefore, the unpoled natural birch bark demonstrates competitive piezoelectric and dielectric properties, surpasses many other biobased materials in its d_{33} value,[16,18,20,67,68] and shows promise for high-frequency piezoelectric applications.

Downloaded from pubs.acs.org/ascecg/article-pdf/14/17/8331/6482052/sc600906.pdf by SOUTHWEST JIAOTONG UNIV user on 07 November 2026

https://doi.org/10.1021/acssuschemeng.6c00906
ACS Sustainable Chem. Eng. 2026, 14, 8331−8341

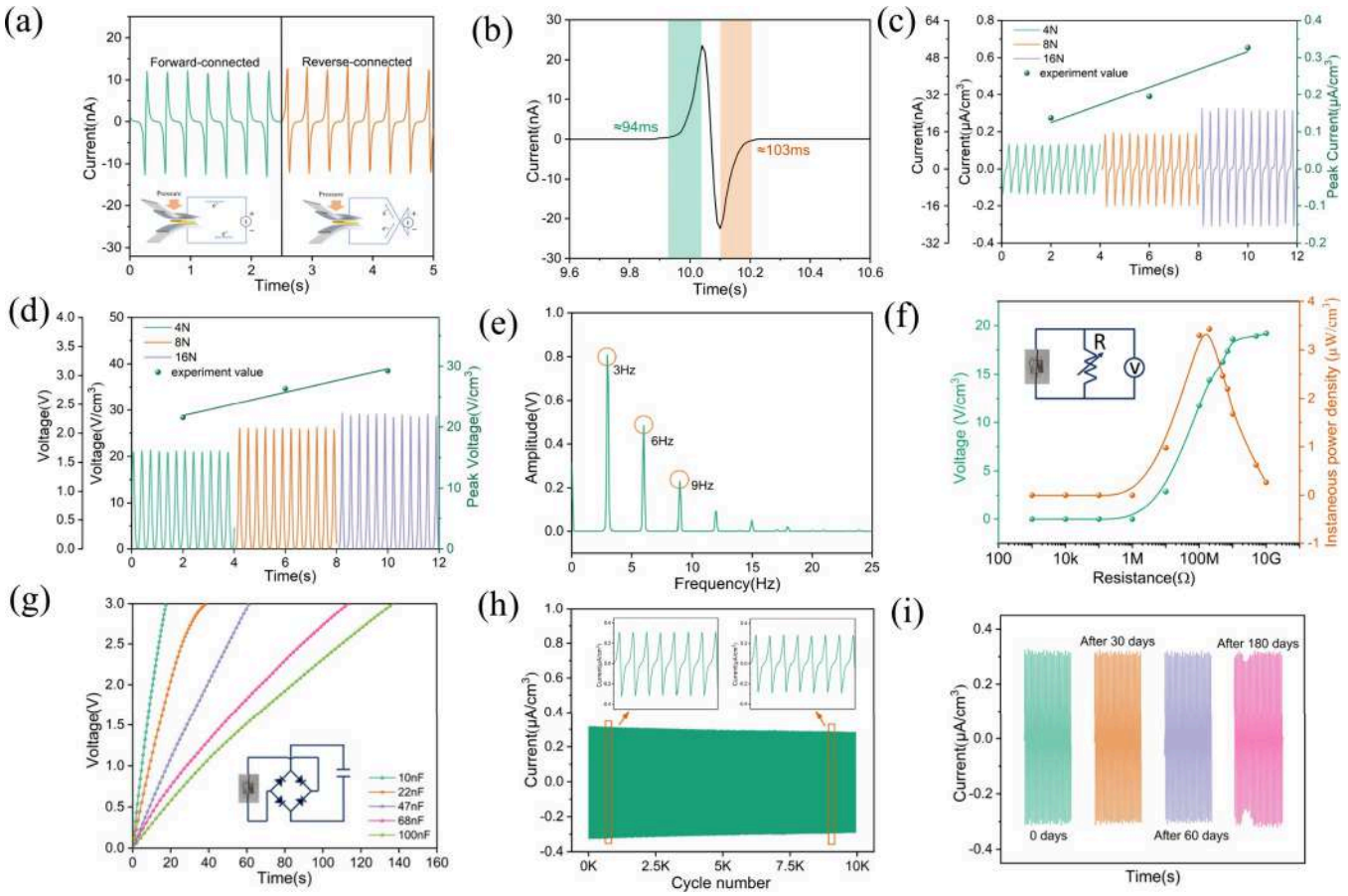


Figure 3. (a) Piezoelectric current signals of BB-PENG in forward and reverse connection modes. (b) Piezoelectric response and recovery times of BB-PENG. (c) Short-circuit current and (d) open-circuit voltage outputs of BB-PENG under a 3 Hz constant impact frequency. (e) Fast Fourier transform spectrum of open-circuit voltage of BB-PENG under a 3 Hz, 16 N impact force. (f) Variation of output voltage and power density of BB-PENG with resistance. (g) Voltage−time curves of BB-PENG charging different commercial capacitors. (h) Stability test of BB-PENG. (i) Piezoelectric signals of the same BB-PENG measured after different storage periods (sealed sample, humidity: ∼50%, temperature: 15−30 °C).

Despite its relatively low cellulose content, the birch bark demonstrates superior piezoelectric properties compared with the trunk, which has a higher cellulose content. This phenomenon is closely associated with the unique component distribution of the birch bark. Specifically, the birch bark is significantly richer in polyphenolic compounds (e.g., tannins) than the birch tree trunk. These polyphenols exert defensive effects against the pathogenic microorganisms and, thus, accumulate in the bark. Polyphenol molecules are rich in phenolic hydroxyl groups, which can form a dense and highly stable intermolecular hydrogen-bonding network with the hydroxyl groups on cellulose chains. Taking the proanthocyanidins of tannins as an example, they can interact with cellulose (Figure 2e). This effectively promotes the oriented arrangement and self-polarization of internal dipoles in natural materials, thereby enhancing the intrinsic polarization intensity and piezoelectric response of white birch bark.

Based on such a phenomenon and structure, the piezoelectric working mechanism for birch bark-based piezoelectric nanogenerator (BB-PENG) is proposed, which is illustrated in Figure 2f. Unlike classical piezoelectric theories based on idealized crystalline structures,[69] the piezoelectric effect in birch bark originates from the orientation of internal molecular dipoles. Initially, without external force, the cellulose crystals with highly oriented dipoles in the birch bark are undeformed and electrically neutral. Upon mechanical stimulation, the active layer deforms, deflecting the aligned dipoles. This reduces the level of net polarization and leads to the generation of a voltage between the electrodes. To neutralize this potential difference, free charges flow rapidly in the circuit, producing a transient current observed macroscopically as the piezoelectric output.

Under an external stimulus, the BB-PENG produces piezoelectric signals, as confirmed by a switching-polarity test (Figure S3 and Figure 3a). Further experiments show that the output is independent of the active area of birch bark, demonstrating that the response originates from the piezoelectric effect rather than the triboelectric effect (Figure S4). It was also confirmed that changes in bark thickness had a relatively small impact on the consistency of piezoelectric output results (Figure S5). Nevertheless, the optimal thickness is 0.2 mm: excessively thin films yield insufficient effective strain, whereas overly thick films increase internal charge migration losses. Figure 3b presents an enlarged view of a complete output current cycle. A response time of ∼94 ms and a recovery time of ∼103 ms demonstrate millisecond-scale energy conversion (Figure S6). The waveform features—a positive surge and a negative plunge—correspond to transient impact deformation and surface charge polarity reversal during recovery (attributed to domain polarization displacement), respectively. This dynamic behavior suggests potential for applications such as impact sensing and transient mechanical

https://doi.org/10.1021/acssuschemeng.6c00906
ACS Sustainable Chem. Eng. 2026, 14, 8331−8341

Downloaded from pubs.acs.org/ascecg/article-pdf/14/17/8331/6482052/sc600906.pdf by SOUTHWEST JIAOTONG UNIV user on 07 November 2026

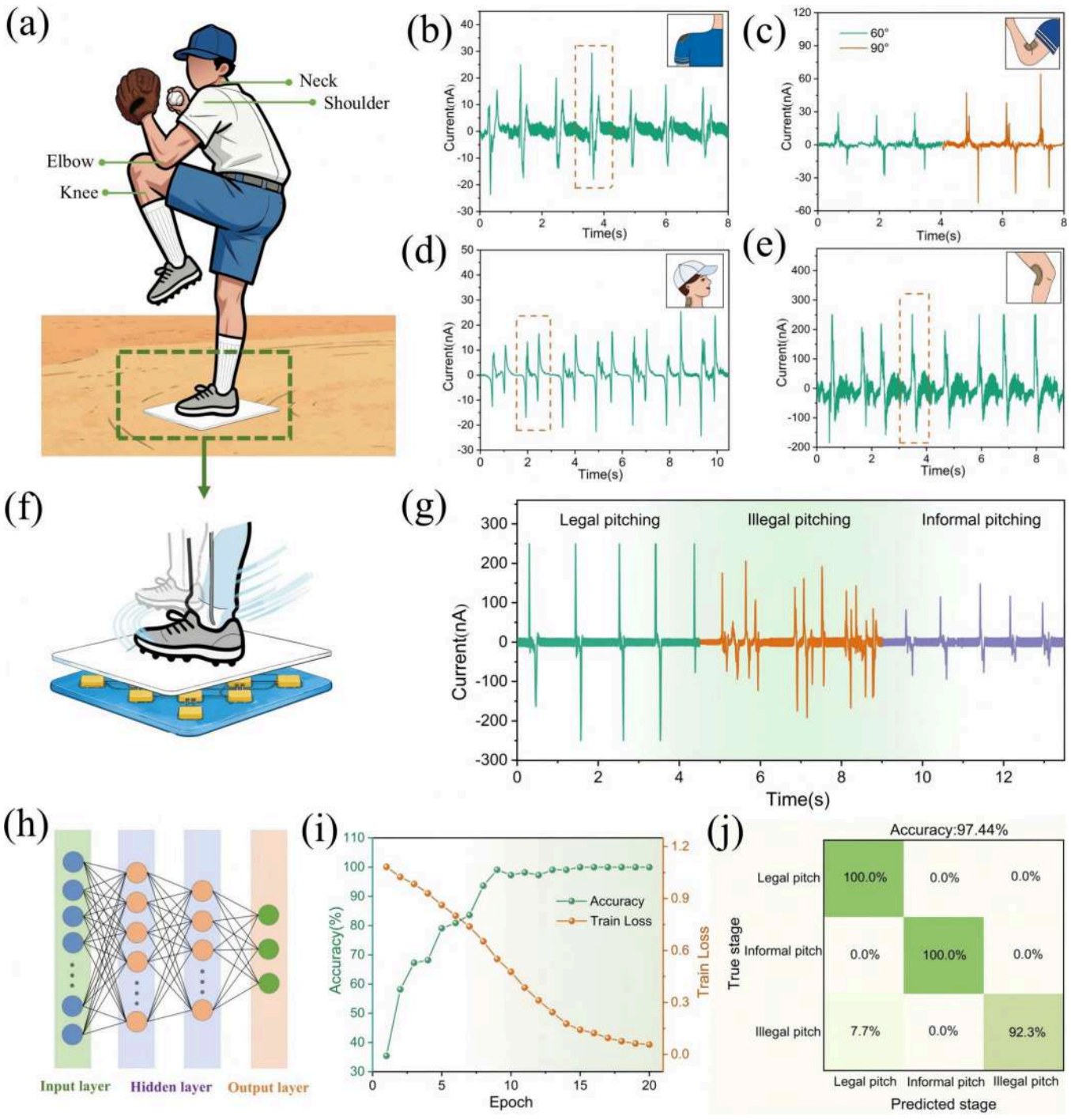


Figure 4. Demonstration of BB-PENG and machine learning-assisted violation recognition in baseball games: (a) schematic diagram of the motion of a baseball pitcher; (b) shoulder torsion; (c) elbow flexion; (d) neck flexion; (e) knee joint flexion; (f) schematic diagram of the machine learning-assisted violation recognition scenario in baseball games; (g) three typical signals (legal pitching, illegal pitching, and informal pitching) obtained serve as the input to the machine learning algorithm; (h) machine learning algorithm of MLP for violation recognition; (i) classification accuracy and loss function of violation recognition based on the training data set; (j) confusion matrix of the signal test data set.

energy harvesting. The selected frequency and force ranges (1−3 Hz,4−16 N) not only align with realistic mechanical excitations in daily human activities to improve practical relevance, but also are consistent with typical parameters reported in the relevant literature to ensure reliable comparability, while enabling clear characterization of the performance trends and their effects on the piezoelectric output.[70,71] Figure 3c,d shows that increasing impact force (4−16 N at 3 Hz) linearly enhances the output of the BB-PENG due to greater mechanical deformation. A maximum current density of 0.33 μA cm^{-3} and a maximum voltage density of 29.3 V cm^{-3} are achieved at a 16 N impulse force, ranking competitively among natural biological material-based nanogenerators (Table S2). Compared with the short-circuit current signal in Figure 3c, the open-circuit voltage signal in Figure 3d exhibits a distinct unipolar characteristic, where the

https://doi.org/10.1021/acssuschemeng.6c00906
ACS Sustainable Chem. Eng. 2026, 14, 8331−8341

Downloaded from pubs.acs.org/ascecg/article-pdf/14/17/8331/6482052/sc600906.pdf by SOUTHWEST JIAOTONG UNIV user on 07 November 2026

negative peak is significantly smaller than the positive peak, whereas the current signal maintains bipolar symmetry. This discrepancy can be attributed to the capacitive nature of the device.[72,73] Birch bark serves as the dielectric layer, and the BB-PENG can be regarded as a parallel-plate capacitor. During the compression stage, piezoelectric charges accumulate at the electrode surfaces, generating a positive voltage; during the release stage, the piezoelectric polarization reverses and the stored charges in the device capacitance partially neutralize the reversed piezoelectric charges, resulting in a substantially attenuated negative voltage. In contrast, the amount of charge transferred during the charging and discharging processes is essentially symmetric; consequently, the current signal retains a bipolar characteristic. Similar electrical output results were also observed on other piezoelectric devices.[19,72,74] The influence of the impact frequency on the piezoelectric output was also examined (Figure S7). The frequency dependence is notably less significant than that induced by the variations in force amplitude. Furthermore, the fast Fourier transform (FFT) is applied to the original time-domain signals (3 Hz, 16 N) to obtain the corresponding frequency-domain spectrum (Figure 3e). The spectrum shows a dominant voltage peak at the fundamental frequency (3 Hz), confirming the efficient conversion of low-frequency mechanical energy by the BB-PENG. Additionally, the presence of harmonic responses indicates the device's sensitivity to broadband mechanical excitations, which is relevant for harvesting ambient low-frequency energy. To evaluate practical power generation, the BB-PENG's output is measured across a range of load resistances under a 3 Hz, 16 N impact. As shown in Figure 3f, the output voltage first increases with load resistance, reaches a maximum of 19.2 V cm^{-3} at 100 MΩ, and then decreases. Correspondingly, the output current decreases with an increasing external load resistance (Figure S8). The calculated instantaneous power density reaches a maximum of 3.42 μW cm^{-3} at a load resistance of 200 MΩ (Figure 3f). The electrical energy generated by the BB-PENG is used to directly power two green LEDs without any external energy storage (Figure S9). To further assess its capability to drive small electronics, the BB-PENG is integrated into a circuit to charge commercial capacitors of various capacitances (Figure 3g). The different capacitors are successfully charged to 3 V within a short time, demonstrating the practical feasibility of the BB-PENG for energy harvesting and storage. Despite the inherent fragility of biological materials, the BB-PENG exhibits excellent durability and stability. Under continuous dynamic stimulation (3 Hz, 16 N, >10,000 cycles), its piezoelectric output shows no significant degradation (Figure 3h), and no structural cracks are observed in the birch bark (Figure S10), confirming robust electromechanical conversion. Furthermore, the device's piezoelectric output remains stable even after prolonged storage at room temperature (Figure 3i), demonstrating strong resistance to environmental factors. Since the device is encapsulated with polyurethane (PU) (Figure 2f), the different humidity conditions have a relatively small impact on the signal stability of the output piezo-signals, although the amplitude of the output piezo-signals shows a slight decrease with increasing relative humidity (Figure S11). These results highlight its potential for long-term, reliable energy harvesting.

Traditional violation detection in sports relies on referees' observation and video replay, which can be subjective and lack real-time capability. To address this issue, particularly for identifying illegal pitching in baseball, we develop a self-powered, flexible tactile sensor using the natural BB-PENG. This wearable device enables real-time objective monitoring of pitcher postures. The pitching motion involves coordinated actions: shoulder torsion, sequential elbow flexion, upward neck flexion, stable pivot foot placement, and knee bend for energy storage, culminating in the pitch (Figure 4a). By attaching the sensor to key body parts, it captures characteristic piezoelectric current signals from shoulder torsion (Figure 4b), varying elbow angles (Figure 4c), neck flexion (Figure 4d), and knee flexion (Figure 4e). Piezoelectric voltage signals can also be used for motion detection (Figure S12). According to baseball rules, pitching requires continuous motion without extraneous movements. To validate this, pivot foot violations are monitored using a BB-PENG sensor on the pitcher's rubber (Figure 4f). As shown in Figure 4g, the three types of characteristic signals correspond to distinct pitching scenarios: (I) legal pitch: the pivot foot maintains continuous contact, producing a single stable pulse. (II) Illegal pitch: characterized by improper foot movement (e.g., repeated lifting), it results in a pulse train with interruptions and periodic fluctuations. (III) Informal motion: refers to tentative adjustments during stance preparation, generating discrete, low-amplitude, short-duration pulses. This category, i.e., informal motion, is key to avoiding false positives from normal movements. The three-level classification system accurately identifies illegal pitches while effectively minimizing the misjudgment common to traditional binary approaches.

Based on the aforementioned classification, we design a rule-augmented neural classification pipeline that integrates domain knowledge-driven feature construction with a lightweight multilayer perceptron (MLP). Concretely, each signal channel is first represented by its raw time-series waveform, which is then enriched with a set of physically interpretable summary features derived from practical engineering decision rules. These rule-aware features include the maximum positive current, minimum (negative) current, and absolute peak magnitude (encoding the degree of conformity between a given signal and the legal pitching, illegal pitching, and informal pitching patterns defined based on underlying current thresholds). By concatenating these rule-informed descriptors with the original waveform vector and performing feature standardization, we obtain a hybrid representation that jointly captures low-dimensional signal dynamics and high-level diagnostic cues. Based on this representation, we train a compact MLP classifier comprising two hidden layers (128 and 64 neurons, respectively) with ReLU activation functions and Dropout regularization, using the Adam optimizer (learning rate 5×10^{-4}) and a cross-entropy loss function (Figure 4h). The data set used in this study comprises 149 biological signal samples divided into 3 categories: legal pitching (49 samples), illegal pitching (50 samples), and informal pitching (50 samples). Each sample consisted of 141 time-step measurements. A stratified split of 75% for training (110 samples) and 25% for testing (39 samples) was adopted with class proportions preserved in both subsets. A fixed random seed was used to ensure reproducibility. In addition to the raw time-series features, nine rule-based features were extracted based on domain-informed amplitude thresholds (50, 100, and 200), resulting in a 150-dimensional feature vector per sample. These threshold values were determined through exploratory data analysis of signal amplitude distributions across the three classes. Despite operating in the small data regime, the proposed model converges within 20 epochs and achieves an

Downloaded from pubs.acs.org/ascecg/article-pdf/14/17/8331/6482052/sc600906.pdf by SOUTHWEST JIAOTONG UNIV user on 07 November 2026

https://doi.org/10.1021/acssuschemeng.6c00906
ACS Sustainable Chem. Eng. 2026, 14, 8331−8341

accuracy of 97.44% and a macro-F1 score of 0.9743 on the test set (Figure 4i). As shown in Figure 4j, the confusion matrix indicates that the model achieves 100% recognition accuracy for the legal pitching and informal pitching conditions with only one misclassification in the illegal pitching class, corresponding to per-class recall rates close to or equal to 100%. These results demonstrate that embedding explicit rule-based features into the neural classifier significantly enhances the model's discriminative power and stability, enabling a simple MLP to deliver near-perfect three-way classification performance with low computational cost and good interpretability. This monitoring system thereby exhibits significant application potential for assisting baseball umpires in violation detection.

CONCLUSIONS

In this work, we demonstrated the piezoelectric effect of birch bark. During the upward growth of the birch tree, the cellulose crystals are induced to form a highly preferred orientation within the bark, which exhibits high electrical performances. Its nanostructure provides numerous stress concentration points, further enhancing the piezoelectric effect. Compared with previously reported natural piezoelectric materials, birch bark exhibits excellent waterproof and mold-resistant properties while enabling large-area fabrication for scalable applications. Moreover, the unpoled birch bark exhibited a piezoelectric coefficient (d_{33}) of 3.09 pm V^{-1}, and the corresponding nanogenerator achieved a piezoelectric voltage output of 29.3 V cm^{-3}, a piezoelectric current output of 0.33 μA cm^{-3}, and a power density of 3.42 μW cm^{-3}. After over 10,000 cycles of mechanical impact (3 Hz, 16 N) or 180 days of storage, the piezoelectric output showed no significant degradation, confirming robust electromechanical conversion. This presents relatively high values compared to those reported for natural piezoelectric materials. As a proof of concept, an integrated foul detection system was further designed by combining the BB-PENG with an MLP classifier. With the assistance of machine learning, the system could accurately identify sports rule violations, offering reliable technical support for referees. This work highlights natural birch bark as a promising green piezoelectric material for self-powered devices in the Era of Artificial Intelligence, paving the way for sustainable energy solutions in smart electronics.

EXPERIMENTAL PROCEDURES

Materials and Reagents

The utilized birch bark was derived from Russian *Betula platyphylla* and purchased from Taoyi Materials Co., Ltd., Shanghai, China. Blue silica gel particles were supplied by Shengda Desiccant Co., Ltd., Suzhou, China. The birch bark was cleaned with distilled water. Then they were buried in the blue silica gel particles for 48 h. Thereafter, the dried birch bark was removed from the silica gel desiccant. Without any further chemical treatment, it was used directly for the device fabrication. This bark is basically a waste part of the birch trees, yet it is a renewable material.

Fabrication of Piezoelectric Nanogenerator

The piezoelectric nanogenerator (PENG) was prepared from intact, dried natural birch bark, aluminum (Al) electrodes, and polyurethane tape (PU), in a sandwich structure, as shown in Figure 2f. First, the two layers of adhesive-backed aluminum films were attached to the top and bottom sides of the birch bark. They were used as electrodes to derive piezoelectric signals. Next, the Al electrodes were encapsulated by using PU tape. Finally, the PENG device was fixed to acrylic (PMMA) plates to ensure a smooth shock during the subsequent piezoelectric measurement. The impact head of the measurement system was also made of the same acrylic resin to eliminate possible interference from triboelectric charges. The prepared birch bark-based piezoelectric nanogenerator (BB-PENG) has an area of 20 × 20 mm and a thickness of 0.42 mm, with a piezo-active layer thickness of 0.2 mm (Figure S13).

Characterization of Materials

Field emission scanning electron microscopy (FE-SEM) was conducted on a JSM7800F PRIME instrument (Japan Electronics Co., Ltd.). Energy-dispersive spectroscopy (EDS) was investigated using an Oxford X-Max 80 spectrometer (Oxford Instruments Ltd.). Attenuated total reflectance Fourier transform infrared (ATR-FTIR) spectra were obtained by using a Nicolet iS20 spectrometer. X-ray diffraction (XRD) data were acquired on a PANalytical X'pert PRO diffractometer. Pole figures were measured by using a PANalytical Empyrean Series 2 X-ray diffraction system. The polar angle α ranged from 0° to 60°, and the azimuthal angle β ranged from 0°to 360°, with a step size of 5° for both α and β. The ferroelectric behavior and piezoelectric properties of the unpoled birch bark were measured by using a TF Analyzer 2000E instrument. The dielectric properties of natural birch bark were investigated using a Dielectric Analyzer (DEA) at room temperature.

ASSOCIATED CONTENT

Supporting Information

The Supporting Information is available free of charge at https://pubs.acs.org/doi/10.1021/acssuschemeng.6c00906.

SEM image of birch bark, EDS spectrum of birch bark, and EDS elemental mapping images of birch bark showing C, O, and Si distributions; SEM and EDS of unwashed birch bark; schematic drawing of the impact measurement system; piezoelectric output of birch bark with different active areas; piezoelectric output of birch bark with different thicknesses; piezoelectric response/recovery time of BB-PENG at different frequencies; open-circuit voltage and short-circuit current of BB-PENG under an 8 N constant impact force and 1, 2, and 3 Hz impact frequencies; output current of the BB-PENG as a function of external load resistance, measured under a 3 Hz, 16 N impact force; digital image of BB-PENG and LEDs connected via a breadboard and digital image demonstrating the instantaneous illumination of the green LEDs, powered by the electrical energy generated by BB-PENG under palm tapping; SEM images of the surface and cross-section of the birch bark after 10,000 cycles of impact; short-circuit current of the birch bark at different humidity levels; output voltage generation from wrist flexion and knee flexion; schematic diagram showing the thickness of each component in the BB-PENG (Figures S1−S13); comparison of the measured ferroelectric response of birch bark with the reported biopiezoelectric materials and comparison of the piezoelectric output of birch-bark device with the reported biological materials based piezoelectric nanogenerators (Tables S1−S2); calculation of total crystallinity of birch bark and measurement method of the piezoelectric coefficient d_{33} (Notes S1 and S2) (PDF)

Downloaded from pubs.acs.org/ascecg/article-pdf/14/17/8331/6482052/sc600906.pdf by SOUTHWEST JIAOTONG UNIV user on 07 November 2026

https://doi.org/10.1021/acssuschemeng.6c00906
ACS Sustainable Chem. Eng. 2026, 14, 8331−8341

AUTHOR INFORMATION

Corresponding Authors

Weiqing Yang − *Research Institute of Frontier Science, Southwest Jiaotong University, Chengdu, Sichuan 610031, China;* orcid.org/0000-0001-8828-9862; Email: wqyang@swjtu.edu.cn

Jun Lu − *School of Chemistry, Southwest Jiaotong University, Chengdu, Sichuan 610031, China;* orcid.org/0000-0002-0606-9565; Email: junluprc@hotmail.com

Authors

Biyao Huang − *School of Chemistry, Southwest Jiaotong University, Chengdu, Sichuan 610031, China*

Chu Pan − *School of Chemistry, Southwest Jiaotong University, Chengdu, Sichuan 610031, China*

Xueyi Li − *Guangdong Institute of Smart Education, Jinan University, Guangzhou, Guangdong 510632, China*

Juan Li − *School of Chemistry, Southwest Jiaotong University, Chengdu, Sichuan 610031, China*

Complete contact information is available at: https://pubs.acs.org/10.1021/acssuschemeng.6c00906

Author Contributions

[#]Other used names were Jun Lv and Jun Lyu.

Notes

The authors declare no competing financial interest.

ACKNOWLEDGMENTS

This work was financially supported by National Natural Science Foundation of China (No. 52073237). The authors would like to thank the Analysis and Testing Center of Southwest Jiaotong University.

REFERENCES

(1) Yin, L.; Kim, K. N.; Lv, J.; Tehrani, F.; Lin, M.; Lin, Z.; Moon, J. M.; Ma, J.; Yu, J.; Xu, S.; Wang, J. A Self-Sustainable Wearable Multi-Modular E-Textile Bioenergy Microgrid System. *Nat. Commun.* **2021**, *12* (1), 1542.

(2) Yu, R.; Feng, S.; Sun, Q.; Xu, H.; Jiang, Q.; Guo, J.; Dai, B.; Cui, D.; Wang, K. Ambient Energy Harvesters in Wearable Electronics: Fundamentals, Methodologies, and Applications. *J. Nanobiotechnol.* **2024**, *22* (1), 497.

(3) Yuan, M.; Zhang, X.; Wang, J.; Zhao, Y. Recent Progress of Energy-Storage-Device-Integrated Sensing Systems. *Nanomaterials* **2023**, *13* (4), 645.

(4) Arya, S.; Sharma, A.; Singh, A.; Ahmed, A.; Dubey, A.; Padha, B.; Khan, S.; Mahadeva, R.; Khosla, A.; Gupta, V. Review—Energy and Power Requirements for Wearable Sensors. *ECS Sens. Plus* **2024**, *3* (2), No. 022601.

(5) Kim, N.; Kim, S.; Ham, S.-H.; Park, J.; Han, M. J.; Kim, M. Chiral Materials in Wearable Sensors: Current Advances and Future Directions. *ACS Sens.* **2025**, *10* (8), 5288−5298.

(6) Zhang, M.; Li, X.; Shen, N.; Zhong, C.; Zhang, Y.; Zhou, S.; Liao, Q.; Qin, L. A Self-Powered Portable Spherical Grip Sensor Based on Flexible PZT Piezoelectric Composites for Rehabilitation Self-Monitoring. *Nano Energy* **2025**, *138*, No. 110906.

(7) Su, Y.; Wang, Q.; Huan, Y.; Wang, J.; Sun, W.; Li, Y.; Wei, T.; Cheng, Z. Concurrently Enhanced Piezoelectric Performance and Curie Temperature in Stressed Lead-Free $Ba_{0.85}Ca_{0.15}Ti_{0.9}Zr_{0.1}O_3$ Ceramics. *Nat. Commun.* **2025**, *16* (1), 4049.

(8) Zhu, Q.; Song, X.; Chen, X.; Li, D.; Tang, X.; Chen, J.; Yuan, Q. A High Performance Nanocellulose-PVDF Based Piezoelectric Nanogenerator Based on the Highly Active CNF@ZnO via Electrospinning Technology. *Nano Energy* **2024**, *127*, No. 109741.

(9) Guerin, S.; Tofail, S. A. M.; Thompson, D. Organic Piezoelectric Materials: Milestones and Potential. *NPG Asia Mater.* **2019**, *11*, 10.

(10) Chorsi, M. T.; Curry, E. J.; Chorsi, H. T.; Das, R.; Baroody, J.; Purohit, P. K.; Ilies, H.; Nguyen, T. D. Piezoelectric Biomaterials for Sensors and Actuators. *Adv. Mater.* **2019**, *31* (1), No. 1802084.

(11) Wang, R.; Sui, J.; Wang, X. Natural Piezoelectric Biomaterials: A Biocompatible and Sustainable Building Block for Biomedical Devices. *ACS Nano* **2022**, *16* (11), 17708−17728.

(12) Karan, S. K.; Maiti, S.; Paria, S.; Maitra, A.; Si, S. K.; Kim, J. K.; Khatua, B. B. A New Insight towards Eggshell Membrane as High Energy Conversion Efficient Bio-Piezoelectric Energy Harvester. *Mater. Today Energy* **2018**, *9*, 114−125.

(13) Ghosh, S. K.; Mandal, D. High-Performance Bio-Piezoelectric Nanogenerator Made with Fish Scale. *Appl. Phys. Lett.* **2016**, *109* (10), No. 103701.

(14) Son, H.-Y.; Park, S.-S. Collagen-Based Biopiezoelectric Nanogenerator Prepared from Pollack Skin. *Mater. Today Sustain.* **2024**, *25*, No. 100689.

(15) Chougale, M. Y.; Khan, M. U.; Kim, J.; Cosgrove, J.; Shaukat, R. A.; Saqib, Q. M.; Banjade, M.; Patil, S. R.; Brown, C.; Dubal, D.; Bae, J. Snake Ecdysis: A Potential e-Material for Advanced Electronic Technology. *Nano Energy* **2023**, *111*, No. 108399.

(16) Kar, E.; Barman, M.; Das, S.; Das, A.; Datta, P.; Mukherjee, S.; Tavakoli, M.; Mukherjee, N.; Bose, N. Chicken Feather Fiber-Based Bio-Piezoelectric Energy Harvester: An Efficient Green Energy Source for Flexible Electronics. *Sustain. Energy Fuels* **2021**, *5* (6), 1857−1866.

(17) Fukada, E. Piezoelectricity of Wood. *J. Phys. Soc. Jpn.* **1955**, *10* (2), 149−154.

(18) Maiti, S.; Kumar Karan, S.; Lee, J.; Kumar Mishra, A.; Bhusan Khatua, B.; Kon Kim, J. Bio-Waste Onion Skin as an Innovative Nature-Driven Piezoelectric Material with High Energy Conversion Efficiency. *Nano Energy* **2017**, *42*, 282−293.

(19) Shao, D.; Wang, C.; Li, W.; Lu, L.; Lu, J.; Yang, W. Natural Ginkgo Tree Leaves as Piezo-Energy Harvesters. *J. Mater. Chem. C* **2022**, *10* (40), 15016−15027.

(20) Qadir, A.; Faraz, S. M.; Mehdi, M. Electromechanical Characterization of Date Fruit Membrane: A Sustainable Material for Bio-Piezoelectric Energy Harvesting. *J. Renewable Sustainable Energy* **2025**, *17* (3), No. 033102.

(21) Bairagi, S.; Ghosh, S.; Ali, S. W. A Fully Sustainable, Self-Poled, Bio-Waste Based Piezoelectric Nanogenerator: Electricity Generation from Pomelo Fruit Membrane. *Sci. Rep.* **2020**, *10* (1), 12121.

(22) Chen, X.; Zhu, Q.; Jiang, B.; Li, D.; Song, X.; Huang, L.; Zhang, Y.; Chen, J.; Yuan, Q. Research Progress of Wood and Lignocellulose in Sustainable Piezoelectric Systems. *Nano Energy* **2024**, *126*, No. 109650.

(23) Ram, F.; Garemark, J.; Li, Y.; Pettersson, T.; Berglund, L. A. Functionalized Wood Veneers as Vibration Sensors: Exploring Wood Piezoelectricity and Hierarchical Structure Effects. *ACS Nano* **2022**, *16* (10), 15805−15813.

(24) Fukada, E. Piezoelectricity as a Fundamental Property of Wood. *Wood Sci. Technol.* **1968**, *2* (4), 299−307.

(25) Hirai, N.; Hirai, N. Studies on Piezoelectric Effect of Wood. *Bull. Shizuoka Univ. For.* **1974**, *3*, 11−77.

(26) Rastogi, S.; Pandey, M. M.; Kumar Singh Rawat, A. Medicinal Plants of the Genus Betula—Traditional Uses and a Phytochemical−Pharmacological Review. *J. Ethnopharmacol.* **2015**, *159*, 62.

(27) Zyryanova, O.; Terazawa, M.; Koike, T.; Zyryanov, V. White Birch Trees as Resource Species of Russia: Their Distribution, Ecophysiological Features, Multiple Utilizations. *Eurasian J. For. Res.* **2010**, *13* (1), 25−40.

(28) Li, C.; Junttila, O.; Heino, P.; Tapio Palva, E. Low Temperature Sensing in Silver Birch (Betula Pendula Roth) Ecotypes. *Plant Sci.* **2004**, *167* (1), 165−171.

(29) Kleczewski, N. M.; Herms, D. A.; Bonello, P. Effects of Soil Type, Fertilization and Drought on Carbon Allocation to Root Growth and Partitioning between Secondary Metabolism and Ectomycorrhizae of Betula Papyrifera. *Tree Physiol.* **2010**, *30* (7), 807−817.

Downloaded from pubs.acs.org/ascecg/article-pdf/14/17/8331/6820526/sc600906.pdf by SOUTHWEST JIAOTONG UNIV user on 07 November 2026

(30) Ferm, A. Birch Production and Utilization for Energy. *Biomass Bioenerg.* **1993**, *4* (6), 391−404.
(31) Boakye, E. A.; Mvolo, C. S.; Stewart, J. Systematic Review: Climate and Non-Climate Factors Influencing Wood Density in the Boreal Zone. *BioResources* **2023**, *18* (4), 8757−8770.
(32) Huang, C.-L.; Lindström, H.; Nakada, R.; Ralston, J. Cell Wall Structure and Wood Properties Determined by Acoustics—a Selective Review. *Holz Roh Werkst.* **2003**, *61* (5), 321−335.
(33) Ekman, R. The Suberin Monomers and Triterpenoids from the Outer Bark of Betula Verrucosa Ehrh. *Holzforschung* **1983**, *37* (4), 205−211.
(34) Huang, T.; Li, D.; Ek, M. Water Repellency Improvement of Cellulosic Textile Fibers by Betulin and a Betulin-Based Copolymer. *Cellulose* **2018**, *25* (3), 2115−2128.
(35) Klügl, J.; Di Pietro, G. The Interaction of Water with Archaeological and Ethnographic Birch Bark and Its Effects on Swelling, Shrinkage and Deformations. *Heritage Sci.* **2021**, *9* (1), 3.
(36) Blondeau, D.; St-Pierre, A.; Bourdeau, N.; Bley, J.; Lajeunesse, A.; Desgagné-Penix, I. Antimicrobial Activity and Chemical Composition of White Birch (*Betula Papyrifera* Marshall) Bark Extracts. *MicrobiologyOpen* **2020**, *9* (1), No. e00944.
(37) Ferreira, J. P. A.; Quilho, T.; Pereira, H. Characterization of Betula Pendula Outer Bark Regarding Cork and Phloem Components at Chemical and Structural Levels in View of Biorefinery Integration. *J. Wood Chem. Technol.* **2017**, *37* (1), 10−25.
(38) Daniel, G.; Filonova, L.; Kallas, Å. M.; Teeri, T. T. Morphological and Chemical Characterisation of the G-Layer in Tension Wood Fibres of Populus Tremula and Betula Verrucosa: Labelling with Cellulose-Binding Module CBM1 Hj Cel7A and Fluorescence and FE-SEM Microscopy. *Holzforschung* **2006**, *60* (6), 618−624.
(39) Dragicević, A.; Kitić, D.; Pavlović, D. Biological Activity of the Birch Leaf and Bark. *Lekovite Sirovine* **2022**, *42* (1), 89−95.
(40) Vedernikov, D. N.; Shabanova, N. Y.; Roshchin, V. I. Change in the Chemical Composition of the Crust and Inner Bark of the Betula Pendula Roth. Birch (Betulaceae) with Tree Height. *Russ. J. Bioorg. Chem.* **2011**, *37* (7), 877−48.
(41) Zhao, Y.; Li, J.; Shi, Z.; Wang, D.; Sun, L.; Wang, J.; Zhao, M.; Zhang, S. Chemical Constituents from the Bark of Betula Pendula and Their Chemotaxonomic Significance. *Biochem. Syst. Ecol.* **2023**, *109*, No. 104677.
(42) Fuchino, H.; Konishi, S.; Satoh, T.; Yagi, A.; Saitsu, K.; Tatsumi, T.; Tanaka, N. Chemical Evaluation of Betula Species in Japan. II. Constituents of *Betula Platyphylla* Var. Japonica. *Chem. Pharm. Bull.* **1996**, *44* (5), 1033−1038.
(43) Hiltunen, E.; Pakkanen, T. T.; Alvila, L. Phenolic Extractives from Wood of Birch (Betula Pendula). *Holzforschung* **2004**, *58* (3), 326−329.
(44) Vinod, M.; Singh, M.; Pradhan, M.; Iyer, S. K.; Tripathi, D. K. Phytochemical Constituents and Pharmacological Activities of Betulaalba Linn. -A Review. *Int. J. PharmTech Res.* **2012**, *4* (2), 643−647.
(45) Pisha, E.; Chai, H.; Lee, I.-S.; Chagwedera, T. E.; Farnsworth, N. R.; Cordell, G. A.; Beecher, C. W. W.; Fong, H. H. S.; Kinghorn, A. D.; Brown, D. M.; Wani, M. C.; Wall, M. E.; Hieken, T. J.; Das Gupta, T. K.; Pezzuto, J. M. Discovery of Betulinic Acid as a Selective Inhibitor of Human Melanoma That Functions by Induction of Apoptosis. *Nat. Med.* **1995**, *1* (10), 1046−1051.
(46) Co, M.; Koskela, P.; Eklund-Åkergren, P.; Srinivas, K.; King, J. W.; Sjöberg, P. J. R.; Turner, C. Pressurized Liquid Extraction of Betulin and Antioxidants from Birch Bark. *Green Chem.* **2009**, *11* (5), 668.
(47) Godina, D.; Makars, R.; Paze, A.; Rizhikovs, J. Analytical Method Cluster Development for Comprehensive Characterisation of Suberinic Acids Derived from Birch Outer Bark. *Molecules* **2023**, *28* (5), 2227.
(48) Ren, M.; Yang, Y.; Rao, H.; Gu, A.; Lei, Y.; Yang, Y. Birch Bark Tar Ornaments: Identification of 2000-Year-Old Beads and Bracelets in Southwest China. *Archaeol. Anthrop. Sci.* **2023**, *15* (12), 186.
(49) Karnaouri, A.; Rova, U.; Christakopoulos, P. Effect of Different Pretreatment Methods on Birch Outer Bark: New Biorefinery Routes. *Molecules* **2016**, *21* (4), 427.
(50) Ostapiuk, A.; Kurach, Ł.; Strzemski, M.; Kurzepa, J.; Hordyjewska, A. Evaluation of Antioxidative Mechanisms In Vitro and Triterpenes Composition of Extracts from Silver Birch (Betula Pendula Roth) and Black Birch (Betula Obscura Kotula) Barks by FT-IR and HPLC-PDA. *Molecules* **2021**, *26* (15), 4633.
(51) Kumar, A.; Korpinen, R.; Möttönen, V.; Verkasalo, E. Suberin Fatty Acid Hydrolysates from Outer Birch Bark for Hydrophobic Coating on Aspen Wood Surface. *Polymers* **2022**, *14* (4), 832.
(52) Xiao, Y. Y.; Li, H. L.; Yu, M. L.; Shi, L. S.; Zeng, J. S.; Liu, M. R. Characterization of Natural Cellulosic Fibers from the Bark of the Edgeworthia Chrysantha Plant. *Int. J. Polym. Anal. Ch.* **2023**, *28* (4), 341−350.
(53) French, A. D. Idealized Powder Diffraction Patterns for Cellulose Polymorphs. *Cellulose* **2014**, *21* (2), 885−896.
(54) Montoya-Escobar, N.; Ospina-Acero, D.; Velásquez-Cock, J. A.; Gómez-Hoyos, C.; Serpa Guerra, A.; Gañan Rojo, P. F.; Vélez Acosta, L. M.; Escobar, J. P.; Correa-Hincapié, N.; Triana-Chávez, O.; Zuluaga Gallego, R.; Stefani, P. M. Use of Fourier Series in X-Ray Diffraction (XRD) Analysis and Fourier-Transform Infrared Spectroscopy (FTIR) for Estimation of Crystallinity in Cellulose from Different Sources. *Polymers* **2022**, *14* (23), 5199.
(55) Hielscher, R.; Schaeben, H. A Novel Pole Figure Inversion Method: Specification of the MTEX Algorithm. *J. Appl. Crystallogr.* **2008**, *41* (6), 1024−1037.
(56) Kitade, S.; Shiroma, K.; Akiba, I.; Sakurai, K. Analysis of Crystal Orientation in Injection-Molded Homo Polypropylene and Polypropylene/Rubber Blends Using Microbeam Pole Figure Measurements. *J. Appl. Polym. Sci.* **2025**, *142* (39), No. e57517.
(57) Wu, X.; Pu, L.; Xu, Y.; Shi, J.; Liu, X.; Zhong, Z.; Luo, S. N. Deformation of High Density Polyethylene by Dynamic Equal-Channel-Angular Pressing. *RSC Adv.* **2018**, *8* (40), 22583−22591.
(58) Nolze, G.; Hielscher, R. Orientations − Perfectly Colored. *J. Appl. Crystallogr.* **2016**, *49* (5), 1786−1802.
(59) Su, C.; Shi, G.; Li, X.; Zhang, X.; Müller, A. J.; Wang, D.; Liu, G. Uniaxial and Mixed Orientations of Poly (Ethylene Oxide) in Nanoporous Alumina Studied by X-Ray Pole Figure Analysis. *Macromolecules* **2018**, *51* (23), 9484−9493.
(60) Verma, S.; Pandey, A.; Dalal, S.; Srivastava, M.; Raman, R. X-Ray Pole Figure Analysis for Orienting TGSM Grown Bulk ZnTe Crystal for Terahertz Device Applications. *J. Mater. Sci. Mater. Electron.* **2023**, *34* (9), 817.
(61) Kiyoto, S.; Sugiyama, J. Histochemical Structure and Tensile Properties of Birch Cork Cell Walls. *Cellulose* **2022**, *29* (5), 2817−2827.
(62) Sadeghifar, H.; Ragauskas, A. Lignin as a UV Light Blocker-a Review. *Polymers* **2020**, *12* (5), 1134.
(63) Koopmann, A.-K.; Schuster, C.; Torres-Rodriguez, J.; Kain, S.; Pertl-Obermeyer, H.; Petutschnigg, A.; Huesing, N. Tannin-Based Hybrid Materials and Their Applications: A Review. *Molecules* **2020**, *25* (21), 4910.
(64) O'Donnell, J.; Guerin, S.; Makam, P.; Cazade, P. A.; Haq, E. U.; Tao, K.; Gazit, E.; Silien, C.; Soulimane, T.; Thompson, D.; Tofail, S. A. M. Atomistic-Benchmarking towards a Protocol Development for Rapid Quantitative Metrology of Piezoelectric Biomolecular Materials. *Appl. Mater. Today* **2020**, *21*, No. 100818.
(65) Kim, S.; Kang, J.; Mun, S.; Seol, D.; Sun, C.; Qiao, H.; Kim, Y. Frequency-Dependent PFM Signal Induced by Surface Adsorbates. *Appl. Surf. Sci.* **2022**, *571*, No. 151281.
(66) Alegria, A.; Colmenero, J. Dielectric Relaxation of Polymers: Segmental Dynamics under Structural Constraints. *Soft Matter* **2016**, *12* (37), 7709−7725.
(67) Karan, S. K.; Maiti, S.; Kwon, O.; Paria, S.; Maitra, A.; Si, S. K.; Kim, Y.; Kim, J. K.; Khatua, B. B. Nature Driven Spider Silk as High

Downloaded from pubs.acs.org/ascecg/article-pdf/14/17/8331/6482052/sc600906.pdf by SOUTHWEST JIAOTONG UNIV user on 07 November 2026

https://doi.org/10.1021/acssuschemeng.6c00906
ACS Sustainable Chem. Eng. 2026, 14, 8331−8341

Energy Conversion Efficient Bio-Piezoelectric Nanogenerator. *Nano Energy* **2018**, *49*, 655−666.
(68) Ghosh, S. K.; Mandal, D. Bio-Assembled, Piezoelectric Prawn Shell Made Self-Powered Wearable Sensor for Non-Invasive Physiological Signal Monitoring. *Appl. Phys. Lett.* **2017**, *110* (12), 123701.
(69) Fukada, E. Piezoelectricity of Biopolymers. *Biorheology* **1995**, *32* (6), 593−609.
(70) Qin, Y.; Wang, X.; Wang, Z. L. Microfibre−Nanowire Hybrid Structure for Energy Scavenging. *Nature* **2008**, *451* (7180), 809−813.
(71) Liu, H.; Zhong, J.; Lee, C.; Lee, S. W.; Lin, L. A Comprehensive Review on Piezoelectric Energy Harvesting Technology: Materials, Mechanisms, and Applications. *Appl. Phys. Rev.* **2018**, *5* (4), No. 041306.
(72) Xu, S.; Yeh, Y.; Poirier, G.; McAlpine, M. C.; Register, R. A.; Yao, N. Flexible Piezoelectric PMN−PT Nanowire-Based Nanocomposite and Device. *Nano Lett.* **2013**, *13* (6), 2393−2398.
(73) Xu, L.; Zhang, Z.; Wang, G.; He, Y.; Zhai, J.; Hu, W.; Chen, L.; Wang, L.; Liu, S.; Wang, Z. L. Capacitive Piezotronics. *Nat. Commun.* **2026**.
(74) Sun, J.; Guo, H.; Ribera, J.; Wu, C.; Tu, K.; Binelli, M.; Panzarasa, G.; Schwarze, F. W. M. R.; Wang, Z. L.; Burgert, I. Sustainable and Biodegradable Wood Sponge Piezoelectric Nanogenerator for Sensing and Energy Harvesting Applications. *ACS Nano* **2020**, *14* (11), 14665−14674.

Downloaded from pubs.acs.org/ascecg/article-pdf/14/17/8331/6482052/sc6c00906.pdf by SOUTHWEST JIAOTONG UNIV user on 07 November 2026

https://doi.org/10.1021/acssuschemeng.6c00906
ACS Sustainable Chem. Eng. 2026, 14, 8331−8341